CHEMISTRY OF MATERIALS
Cite This: Chem. Mater. 2019, 31, 9750–9758
Article
pubs.acs.org/cm

Thermal Stability of the Black Perovskite Phase in Cesium Lead Iodide Nanocrystals Under Humid Conditions

Cherrelle J. Thomas,[†,⊥] Yangning Zhang,[†,⊥] Adrien Guillaussier,[†] Khaled Bdeir,[†,∥] Omar F. Aly,[†] Hyun Gyung Kim,[†] Jungchul Noh,[†] Lauren C. Reimnitz,[†] Junjie Li,[§] Francis Leonard Deepak,[§] Detlef-M. Smilgies,[‡] Delia J. Milliron,[†] and Brian A. Korgel*[,†]

[†]McKetta Department of Chemical Engineering and Texas Materials Institute, The University of Texas at Austin, Austin, Texas 78712, United States

[‡]Cornell High Energy Synchrotron Source (CHESS), Cornell University, Ithaca, New York 14853, United States

[§]Nanostructured Materials Group, Department of Advanced Electron Microscopy, Imaging, and Spectroscopy, International Iberian Nanotechnology Laboratory (INL), Av. Mestre José Veiga s/n, 4715-330 Braga, Portugal

[∥]Baha and Walid Bassatne Department of Chemical Engineering, American University of Beirut, Beirut 1107 2020, Lebanon

Supporting Information

ABSTRACT: The equilibrium phase of cesium lead iodide ($CsPbI_3$) at room temperature is yellow and optically inactive due to its indirect band gap. The metastable black phase of $CsPbI_3$ on the other hand exhibits optical properties that are suitable for photovoltaic and light-emitting devices. Here, we examine the stability of the black phase of ligand-stabilized $CsPbI_3$ nanocrystals heated in humid air. Water vapor is known to catalyze the transition of $CsPbI_3$ from the black phase to the yellow phase. Uniform nanocrystals with cube shape were synthesized with capping ligand mixtures of oleylamine and oleic acid or diisooctylphosphinic acid, assembled into superlattices with preferred crystal orientation, and studied using grazing incidence small- and wide-angle X-ray scattering with in situ heating. The black-phase nanocrystals are found to inhabit the γ-orthorhombic phase and do not revert to the equilibrium yellow δ-orthorhombic phase until reaching a relatively high temperature, between 170 and 200 °C, coinciding with superlattice degradation.

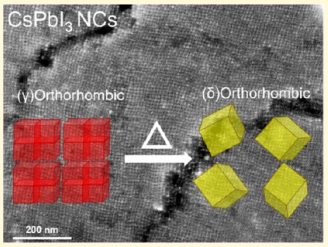

INTRODUCTION

The discovery that organic−inorganic hybrid materials like $CH_3NH_3PbI_3$ and $CH_3NH_3PbI_2Cl$ can make efficient solution-processed solar cells has led to intense interest in lead halide perovskites.[1−3] They have now been used to make solar cells with record device efficiencies that rival single crystal silicon.[4] They are also excellent light emitters.[5] However, the organic moiety (i.e., CH_3NH_3) provides poor thermal and chemical stabilities, and more robust, all-inorganic lead halides with solution processability and good device performance have been sought.[6−8]

Of the possible all-inorganic lead halide perovskites, $CsPbI_3$ has the lowest band gap and makes a good choice for solar cell applications.[6] Its band gap of 1.7 eV is a little high to compete with hybrids in terms of single junction photovoltaic (PV) device efficiency but is well matched with silicon device layers for tandem cells.[9−11] However, the equilibrium phase of $CsPbI_3$ at room temperature is not a perovskite—it is an "optically inactive" δ-orthorhombic phase, which is yellow in color with an indirect band gap that makes it a weak light absorber and poor light emitter.[12−16] A black, optically active phase with a perovskite structure can be made by heating yellow $CsPbI_3$ above a transition temperature of about 330 °C to the α-cubic phase and then rapidly quenching it to room temperature.[13,16] This metastable black material is quite stable in the absence of water vapor even though it is out of equilibrium. Chemical additives, strain engineering, and surface passivation have also been used to help stabilize the black phase. In fact, $CsPbI_3$ has been used to make light-emitting diodes, lasers, and PV devices.[17−28] Black $CsPbI_3$ films with tetragonal phase (β-$CsPbI_3$) were also recently used to fabricate solar cells with power conversion efficiencies of 18.4%.[8] However, humidity catalyzes the rapid transformation of black $CsPbI_3$ to the equilibrium yellow phase.[8,16]

Colloidal synthesis can yield ligand-stabilized $CsPbI_3$ nanocrystals directly in the black perovskite phase without the need for any postsynthesis heating or thermal quenching.[18,19] These nanocrystals are bright light emitters and can be deposited on substrates and processed into photovoltaic devices with device efficiencies as high as 13.4%.[20] Black $CsPbI_3$ nanocrystals are very stable even in the presence of humidity because of the protective, hydrophobic capping ligand layer, but when ligands are removed, the nanocrystals become very susceptible to degradation to the yellow phase just like bulk films and crystals.[29]

Here, we use grazing incidence small- and wide-angle X-ray scattering (GISAXS and GIWAXS) to investigate the crystal structure and thermal stability of ligand-stabilized black-phase

Received: August 29, 2019
Revised: November 6, 2019
Published: November 7, 2019

DOI: 10.1021/acs.chemmater.9b03533
Chem. Mater. 2019, 31, 9750–9758

$CsPbI_3$ nanocrystals. The nanocrystals are made of uniform size and a cube shape and could be assembled into superlattices with orientational order. GIWAXS measurements of these crystallographically oriented nanocrystal films provided two-dimensional (2D) spot patterns that could be used to differentiate between the γ-orthorhombic and α-cubic crystal structures. The γ-phase of $CsPbI_3$ has a perovskite crystal structure composed of linked lead iodide octahedra similar to the α-cubic phase with an orthorhombic distortion. The yellow nonperovskite δ-orthorhombic phase is composed of linear chains of lead and iodide.[16] The nanocrystals retain the black phase when heated in humid air, until reaching 150−200 °C. The phase transition was also monitored optically using in situ photoluminescence (PL) spectroscopy. The black phase of ligand-stabilized $CsPbI_3$ nanocrystals is much more stable than in thin films or bulk crystals. There is no appreciable difference in thermal stability observed for $CsPbI_3$ nanocrystals synthesized with oleylamine (OAm) and oleic acid (OA) or diisooctylphosphinic acid (DIOP).

EXPERIMENTAL DETAILS

Materials. Lead iodide (PbI_2, 99.999% trace-metal basis), cesium carbonate (Cs_2CO_3, 99.9% trace-metal basis), octadecene (ODE, 90%), oleylamine (OAm, 70%), oleic acid (OA, 90%), bis(6-methylheptyl)-phosphinic acid (diisooctylphosphinic acid, DIOP, $C_{16}H_{35}O_2P$, 90%), anhydrous *n*-hexane (95%), anhydrous methyl acetate (99.5%), and anhydrous chloroform (≥99%) were obtained from Sigma-Aldrich. All chemicals were used without further purification.

Nanocrystal Synthesis. $CsPbI_3$ nanocrystals were synthesized with OAm and OA as described by Protesescu et al.[19] or OAm and DIOP as described by Wang et al.[30] Stock solutions of 0.06 M Cs-oleate and Cs-diisooctylphosphinate were made by combining 2.5 mmol of Cs_2CO_3 (0.814 g, 2.5 mmol), 40 mL of ODE, and 2.5 mL (7.8 mmol) of OA or 2.5 mL (7.9 mmol) of DIOP in a three-neck 100 mL flask on a Schlenk line. The solutions were degassed under vacuum (∼150 mTorr) at 120 °C for 1 h and heated at 150 °C under N_2 until the solutions became clear. The stock solutions were stored in a glovebox prior to use.

The nanocrystal synthesis was carried out in a 100 mL three-neck flask on a Schlenk line. First, 0.88 mmol (406 mg) of PbI_2 and 20 mL of ODE were degassed under vacuum (∼150 mTorr) at 120 °C for 1 h. After blanketing with N_2, 2 mL each of OAm and OA (or OAm and DIOP) was added. The reaction mixture was again placed under vacuum (∼150 mTorr), degassed for 30 min at 120 °C, blanketed with N_2, and heated to the desired reaction temperature of 160 °C. Cs-oleate or Cs-diisooctylphosphinate was then added to this reaction mixture by hot injection with a syringe of 3.2 mL of 0.06 M Cs-oleate or Cs-DIOP stock solution heated to 100 °C. The reaction mixture was then cooled after only 5 s to room temperature by immersion in an ice bath.

In a glovebox, 30 mL of methyl acetate was added to the crude reaction mixture. The nanocrystals were precipitated by centrifugation at 8000 rpm (8228*g*) for 5 min. The supernatant was discarded. The nanocrystals were redispersed in 10 mL of anhydrous *n*-hexane and centrifuged again at 8500 rpm (9289*g*) for 5 min to remove all poorly capped nanocrystals. The supernatant was decanted into a vial and stored in a glovebox. The vial was wrapped with aluminum foil and stored in a refrigerator to maintain inert, cold, and dark conditions.

Nanocrystal Superlattice Assembly. Nanocrystals were deposited on Si substrates or transmission electron microscopy (TEM) grids in a glovebox. Si substrates were cut pieces of a 650 μm thick p-type Si wafer (University Wafer), and TEM grids were 200-mesh nickel grids with a continuous carbon coating (Electron Microscopy Sciences). The substrate or TEM grid was placed at the bottom of a 4.5 mL vial. Either hexane or chloroform was used as the dispersing solvent for the assembly. In both cases, 40 μL of $CsPbI_3$ nanocrystal dispersion (6.7 mg mL^{-1} in hexane) was placed on the substrate. For

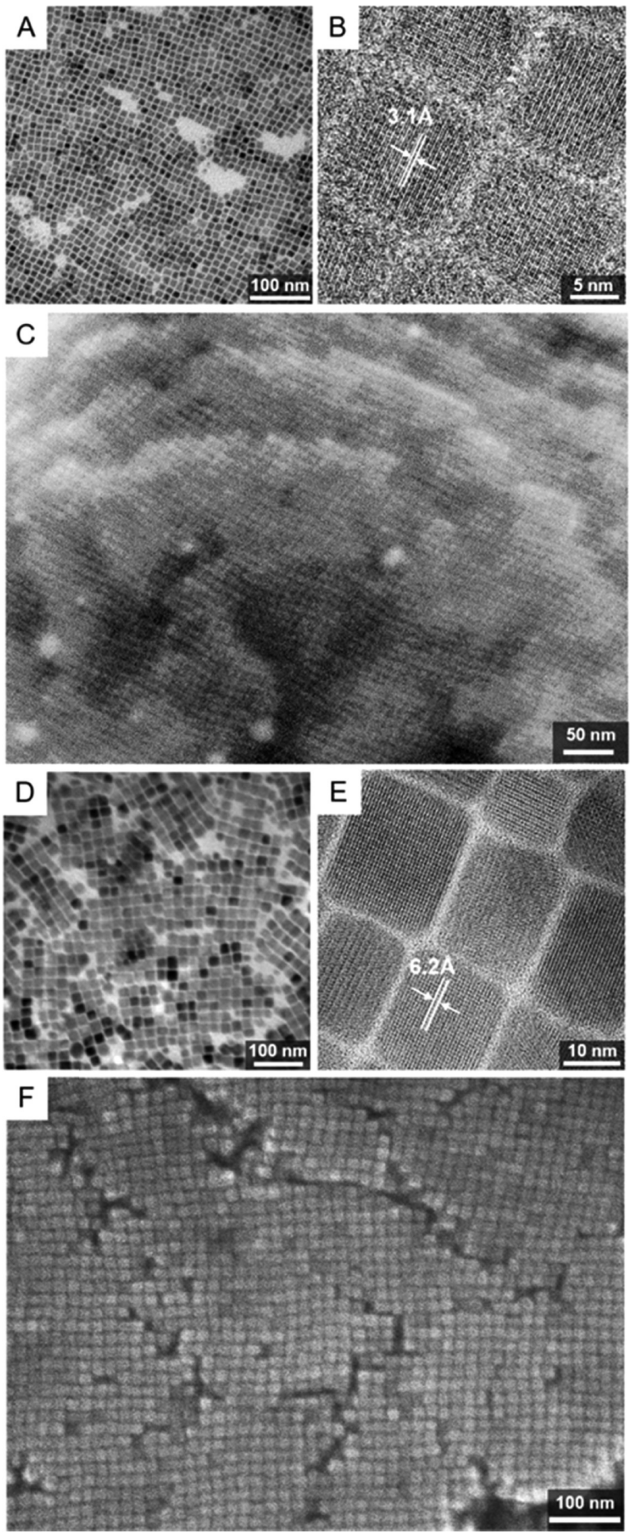

Figure 1. (A, B) TEM and (C) SEM images of $CsPbI_3$ nanocrystals synthesized with OAm and OA. The nanocrystals have a cube shape with an average side length of 8.6 ± 1.5 nm. The lattice spacing of 3.1 Å shown in (B) corresponds to the $\gamma\{220\}$ or $\gamma\{004\}$ planes, depending on whether the nanocrystal is oriented on a $\gamma\{002\}$ or $\gamma\{110\}$ facet. (D, E) TEM and (F) SEM images of $CsPbI_3$ nanocrystals synthesized with OAm and DIOP. The nanocrystals are cube-shaped with an average side length of 17.5 ± 2.8 nm. The lattice spacing of 6.2 Å shown in (E) corresponds to either the $\gamma\{002\}$ or $\gamma\{110\}$ planes, depending on whether the nanocrystal is oriented on a $\gamma\{110\}$ or $\gamma\{002\}$ facet.

DOI: 10.1021/acs.chemmater.9b03533
Chem. Mater. 2019, 31, 9750−9758

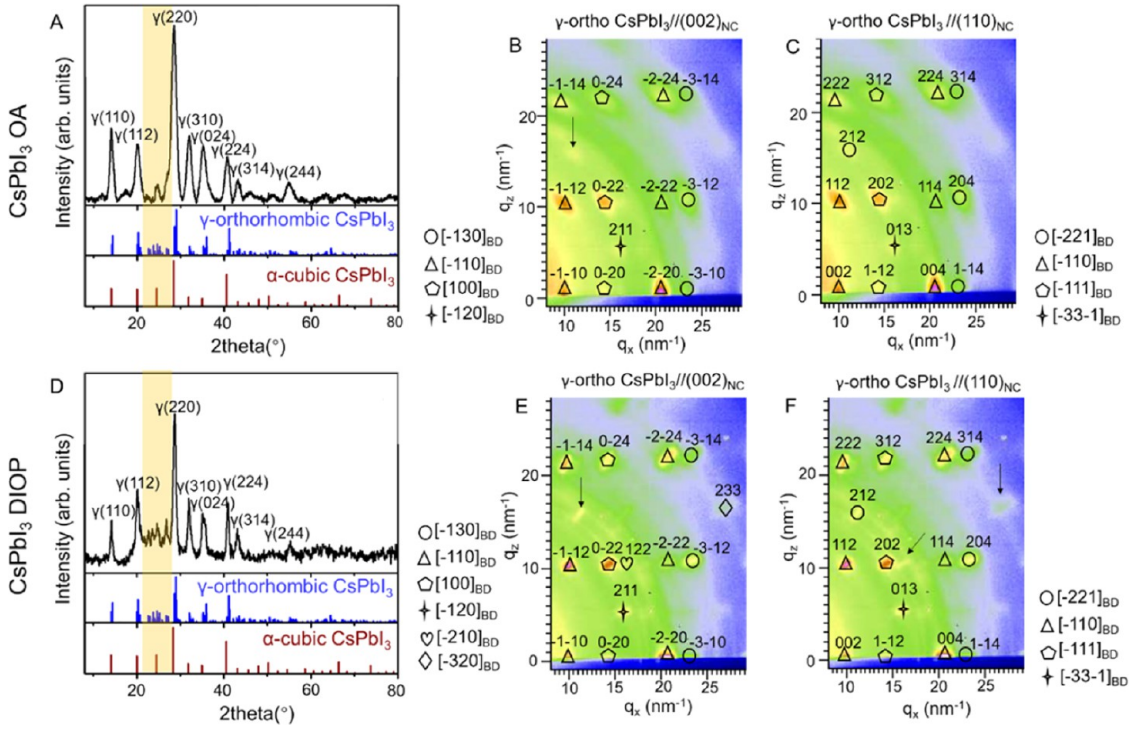

Figure 2. (A) Powder XRD and (B, C) GIWAXS of superlattices of $CsPbI_3$ nanocrystals made with OAm and OA. (D) Powder XRD and (E, F) GIWAXS of superlattices of $CsPbI_3$ nanocrystals made with OAm and DIOP. The shaded regions in (A) and (D) highlight the weak diffraction peaks characteristic of the γ-orthorhombic phase. (B) and (C), or (E) and (F), show the same GIWAXS patterns indexed to two different crystal orientations of γ-$CsPbI_3$. The associated beam directions (BD) needed to account for all of the diffraction spots are provided next to each image. These BD all run parallel to the crystal plane oriented parallel to the substrate. The arrows indicate spots that cannot be indexed for the stated crystal orientation. Indexation details for the GIWAXS data are provided in Tables S1 and S2 in the Supporting Information.

the use of hexane as the dispersing solvent during the assembly, an additional 240 μL of anhydrous hexane was added. For deposition from chloroform, the initial 40 μL of solvent was evaporated, and then the nanocrystals were redispersed with 240 μL of anhydrous chloroform and then dried. The solvent was allowed to evaporate for at least 24 h prior to characterization.

Material Characterization. Nanocrystals were imaged by transmission electron microscopy (TEM) using an FEI Tecnai G2 Spirit BioTwin TEM or a JEOL 2010F TEM operated at 80 or 200 kV accelerating voltage, respectively. Scanning electron microscopy (SEM) imaging of nanocrystal films on Si substrates was carried out with a Zeiss Supra 40 VP SEM with a 4 kV accelerating voltage using the in-lens detector. The samples were electrically grounded using copper tape. Powder X-ray diffraction (XRD) data were obtained from nanocrystals on glass slides on a Rigaku R-axis Spider diffractometer with Cu Kα radiation (λ = 1.541 Å) operated at 40 kV and 40 mA. Data were collected for 10 min with sample rotation at 5° s^{-1}, background-subtracted, and analyzed using 2DP and JADE software. Photoluminescence (PL) emission spectra were acquired from spin-coated films of $CsPbI_3$ nanocrystals on glass slides using a Fluorolog-3 spectrophotometer (Horiba Jobin Yvon) equipped with an in situ heating and temperature control.

Grazing Incidence Small- and Wide-Angle X-ray Scattering (GISAXS and GIWAXS). GISAXS and GIWAXS measurements were performed simultaneously on the D1 beam line at the Cornell High Energy Synchrotron Source (CHESS). Nanocrystal films deposited on Si substrates were heated on a temperature-controlled stage in humid air (40–42% RH) from 23 to 300 °C at a rate of 20 °C min^{-1} from 23 to 100 °C and then 10 °C min^{-1} from 100 to 300 °C. The incident beam angle was 0.25° with a wavelength of 0.929 Å. GISAXS data were collected using a Pilatus 200k detector (487 × 407 pixels with a pixel size of 172 μm × 172 μm) with a sample-to-detector distance of 1.31 m. GIWAXS data were collected using a Pilatus 100k detector (487 × 195 pixels with a pixel size of 172 μm × 172 μm) with a sample-to-detector distance of 105.75 mm. Image processing and peak indexing considering the Ewald sphere distortion of the GIWAXS data were done using FIT2D (version: 12_077_i686_WXP) and indexGIXS-2M software.[31,32]

RESULTS AND DISCUSSION

$CsPbI_3$ Nanocrystal Synthesis, Crystal Phase, and Superlattice Assembly. $CsPbI_3$ nanocrystals were synthesized by hot injection ionic metathesis reactions in octadecene (ODE) using oleylamine (OAm) as a capping ligand with oleic acid (OA) or diisooctylphosphinic acid (DIOP) as complexing agents for Cs^+.[19,30]

$$2Cs(RCOO) + 3PbI_2 \xrightarrow[OA,OAm,ODE]{160°C,5s} 2CsPbI_3 + Pb(RCOO)_2 \quad (1)$$

$$2Cs(R_2PO_2) + 3PbI_2 \xrightarrow[OA,OAm,ODE]{160°C,5s} 2CsPbI_3 + Pb(R_2PO_2)_2 \quad (2)$$

In eqs 1 and 2, RCOO is oleate and R_2PO_2 is diisooctylphosphinate. Nanocrystals were made for the study using OAm with OA or DIOP to determine if there is any noticeable difference in stability using a different capping ligand combination. OA is widely used for the synthesis of perovskite nanocrystals.[19] In one study, Jasieniak and colleagues replaced OA with the dialkyl phosphinic acid, bis-(2,2,4-trimethylpentyl)phosphinic acid, to improve dispersion stability.[30] We examined the relative thermal stability of $CsPbI_3$ nanocrystals made using OA or the phosphinic acid, DIOP. The nanocrystals were purified by precipitation with methyl acetate as the antisolvent.[18] The antisolvent cannot desorb the capping ligand layer or the nanocrystals will rapidly turn yellow.

DOI: 10.1021/acs.chemmater.9b03533
Chem. Mater. 2019, 31, 9750–9758

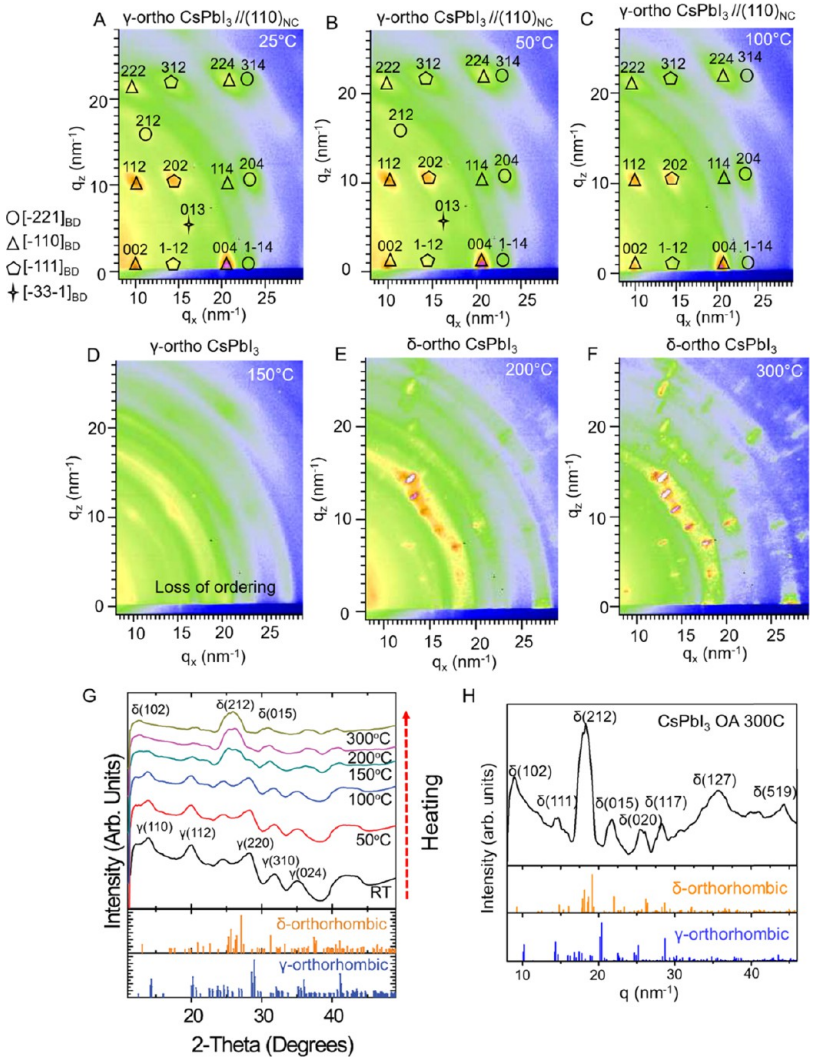

Figure 3. (A–F) GIWAXS data for superlattices of $CsPbI_3$ nanocrystals made with OAm and OA with in situ heating. The patterns are indexed to the γ-orthorhombic phase with the $\gamma(110)$ planes oriented parallel to the substrate. BD indicates the beam direction corresponding to the peak indexing. (G) Radial integration of the GIWAXS patterns in (A–F). (H) Radial integration of the GIWAXS pattern in (F).

Figure 1 shows the TEM and SEM images of the nanocrystals used in the study. They have a cube shape and are slightly elongated with an average aspect ratio of 1.2. The nanocrystals made with OA are smaller than those made with DIOP, with average side lengths of 8.6 ± 1.5 and 17.5 ± 2.8 nm, respectively. The nanocrystals are sufficiently uniform to be assembled into superlattices with a simple cubic structure. The superlattices were used to study the atmospheric stability of the black perovskite phase of the $CsPbI_3$ nanocrystals with heating.

Figure 2 shows the room-temperature XRD and GIWAXS data of $CsPbI_3$ synthesized with OAm and OA or DIOP. The powder XRD patterns in Figure 2A,D exhibit prominent peaks overlapping with both α-cubic and γ-orthorhombic perovskite phases, but with additional weak diffraction features characteristic of γ-$CsPbI_3$. This is consistent with the fact that the nanocrystals are black with bright red fluorescence. GIWAXS patterns in Figure 2B,C,E,F are indexed to γ-orthorhombic $CsPbI_3$ with space group *Pbnm* (no. 60) and lattice parameters a = 8.646 Å, b = 8.818 Å, and c = 12.520 Å.[15] Indexation trials with α-cubic phase cannot account for all of the spots in the patterns (see the Supporting Information Figure S1), i.e., there are a few additional spots that can only be indexed to γ-orthorhombic phase. The orientational order in the superlattice and the GIWAXS measurement technique provides additional scattering information that reveals the nanocrystals to be γ-$CsPbI_3$. The specific $CsPbI_3$ crystal orientations on the substrate are reflected as distinct spots or texture in the diffraction patterns (as opposed to rings). This is similar to orientationally ordered superlattices of cube-shaped nanocrystals of $CH_3NH_3PbI_3$ and $Cs_2AgBiBr_6$ studied recently by GIWAXS.[33,34] Indexation of the pattern indicates that the nanocrystal facets are $\gamma\{110\}$ and $\gamma\{002\}$ surfaces (equivalent to cubic $\alpha\{100\}$ crystal planes with a slight distortion). Note that the patterns can be indexed to the cubic phase, except for the $\gamma(212)$, $\gamma(013)/211$, $\gamma(122)$, and $\gamma(233)$ spots, which are unique to the γ-orthorhombic phase due to its lower symmetry.

The lattice spacing of 3.1 Å shown in the TEM image in Figure 1B corresponds to $\gamma\{220\}$ or $\gamma\{004\}$ planes depending on whether the nanocrystal is oriented on a $\gamma\{002\}$ or $\gamma\{110\}$ facet. The lattice spacing of 6.2 Å shown in Figure 1E corresponds to the $\gamma\{002\}$ or $\gamma\{110\}$ planes depending on whether the nanocrystal is oriented on a $\gamma\{110\}$ or $\gamma\{002\}$ facet. Most probably, the nanocrystals are oriented randomly on $\gamma\{110\}$ and $\gamma\{002\}$ facets, and the GIWAXS data are composed of two

DOI: 10.1021/acs.chemmater.9b03533
Chem. Mater. 2019, 31, 9750–9758

overlapping spot patterns for nanocrystals with these two different orientations on the substrate.[33,34]

Thermal Stability of Black $CsPbI_3$ Nanocrystals in Humid Air. Superlattices of γ-$CsPbI_3$ nanocrystals were heated under atmospheric conditions with a relative humidity of 40−42% while gathering in situ GIWAXS and GISAXS data (Figures 3−6). Figure 3A shows the room-temperature GIWAXS data for $CsPbI_3$ nanocrystals synthesized using OAm and OA with indexing provided only for nanocrystals oriented with $\gamma(110)$ facets on the substrate for clarity. The room-temperature GISAXS data in Figure 4A shows that the

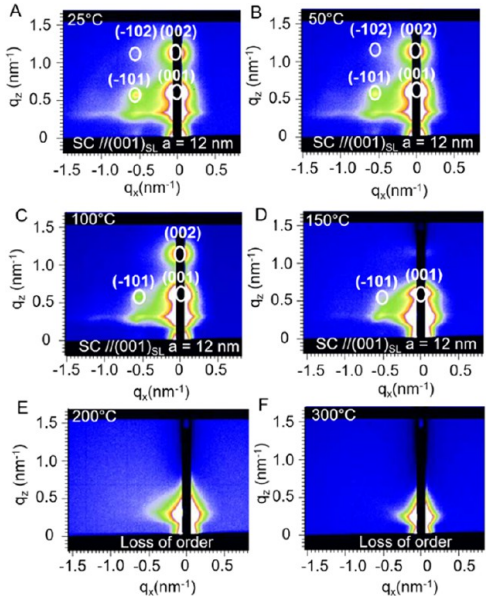

Figure 4. GISAXS of superlattices of $CsPbI_3$ nanocrystals made with OAm and OA with in situ heating at (A) 25 °C, (B) 50 °C, (C) 100 °C, (D) 150 °C, (E) 200 °C, and (F) 300 °C. Diffraction spots are indexed to a simple cubic (SC) superlattice with lattice parameter a_{SL} = 12 nm with a $(001)_{SL}$ orientation on the substrate.

superlattice is a simple cubic structure with a (001) superlattice orientation on the substrate. This orientation is dictated by the cube shape of the nanocrystals and the interactions between the flat crystal facets between neighboring particles and the substrate. The lattice constant of the superlattice is a_{SL} = 12 nm, indicating that there is an interparticle edge-to-edge separation of 3.4 nm. $CsPbBr_3$ nanocrystal superlattices were recently reported with a_{SL} = 12.5 nm with an interparticle edge-to-edge separation of 2.3 nm.[35]

The γ-phase of the nanocrystals is stable up to at least 150 °C. At 150 °C, the GIWAXS pattern still indexes to the γ-phase (Figure 3D) but the spot pattern has degraded to rings, indicating that the nanocrystals lose their orientational order on the substrate, which still retains the γ-phase. This is consistent with the GISAXS data, as the range of order in the superlattice indicated by the GISAXS pattern in Figure 4D is significantly lower than in Figure 4A at room temperature. Figure 3E shows that the nanocrystals have converted to the yellow δ-orthorhombic phase (space group *Pnma*, lattice parameters a = 10.458 Å, b = 4.802 Å, and c = 17.776 Å, PDF #01-076-8587) when the temperature has reached 200 °C. Radial integration of the GIWAXS patterns at 200 and 300 °C in Figure 3G,H matches the expected diffraction pattern of the δ-phase (see the Supporting information, Figures S2 and S3 for the indexation of 2D GIWAXS pattern at 200 and 300 °C). After the γ-to-δ phase transition, there is no specific crystal orientation remaining in the film. GISAXS of the assembly, shown in Figure 4, reveals that much of the out-of-plane superlattice order is indeed lost by 150 °C and that the superlattice structure completely disintegrates by 200 °C. The complete loss of superlattice order in the GISAXS data at 200 °C corresponds with the formation of the δ-orthorhombic phase. It is not clear if the loss of superlattice integrity leads to the phase change or the phase change leads to the loss of the superlattice, but we believe that the degradation is related to the loss of surface capping ligands. Thermogravimetric analysis (TGA) shows that most of the capping ligands have desorbed from the nanocrystals after reaching 350 °C (Supporting Information Figure S5). SEM images of the nanocrystals after heating to 190 °C in humid air also show that the nanocrystals have aggregated into larger particles and recrystallized into nanowires (Supporting Information Figure S6). These SEM data are consistent with the degradation of superlattice by 200 °C observed in GISAXS. Many other kinds of superlattices of ligand-capped nanocrystals degrade near 200 °C due to the loss of bonding of the ligand to the inorganic nanocrystal core. For example, alkanethiol-capped gold nanocrystal superlattices degrade at 190−200 °C when the thiol−gold bond becomes unstable.[36] And superlattices of PbSe nanocrystals capped with trioctylphosphine also degrade in this temperature range.[37] When cooled back to room temperature, the $CsPbI_3$ sample retains its yellow nonperovskite phase.

Figures 5 and 6 show the GIWAXS and GISAXS data for the heated superlattices of $CsPbI_3$ nanocrystals made with OAm and DIOP. These nanocrystals are about twice as large as those made with OAm and OA. The room-temperature GISAXS pattern (Figure 6A) indexes to a simple cubic superlattice structure with a (001) superlattice orientation on the substrate and a lattice constant of a_{SL} = 21 nm, corresponding to an interparticle edge-to-edge separation of 3.5 nm. Indexing of the GIWAXS patterns in Figure 5 is only shown for the $\gamma\{002\}$ orientation for clarity. This leads to a missing spot that can only be indexed to the $\gamma\{110\}$ orientation, which is provided in red, i.e., $\gamma(212)$. The γ-orthorhombic diffraction pattern in the GIWAXS data is retained upon heating up to 200 °C. Although a spot pattern remains, there is a noticeable loss of orientational order once the temperature reaches 150 °C. In the GISAXS data (Figure 6D), the superlattice order is completely gone by 150 °C. Similar to the $CsPbI_3$ nanocrystals made with OAm and OA, these nanocrystals appear to lose orientational and superlattice orders during heating at around 150 °C below the phase change temperature from γ-$CsPbI_3$ to δ-$CsPbI_3$ at about 200 °C. Radial integration of GIWAXS patterns in Figure 5G,H shows the coexistence of γ-$CsPbI_3$ and δ-$CsPbI_3$ phases at 300 °C (2D indexation in the Supporting information, Figure S4).

Optical Properties of Heated γ-$CsPbI_3$ Nanocrystals. Figure 7 shows the PL emission spectra for a film of γ-$CsPbI_3$ nanocrystals made with OAm and OA that were acquired in situ while heating through the γ-to-δ phase transition. At 25 °C, the film exhibits an emission peak centered at 679 nm (1.83 eV). The room-temperature PL peak for the γ-$CsPbI_3$ nanocrystals made with DIOP occurs at a slightly longer wavelength of 698 nm (1.78 eV), consistent with their larger size and reduced quantum confinement-related shifting of the optical gap. The PL peak intensity gradually decreases as the temperature goes up. The drop in PL intensity is also observed visually, as in

DOI: 10.1021/acs.chemmater.9b03533
Chem. Mater. 2019, 31, 9750−9758

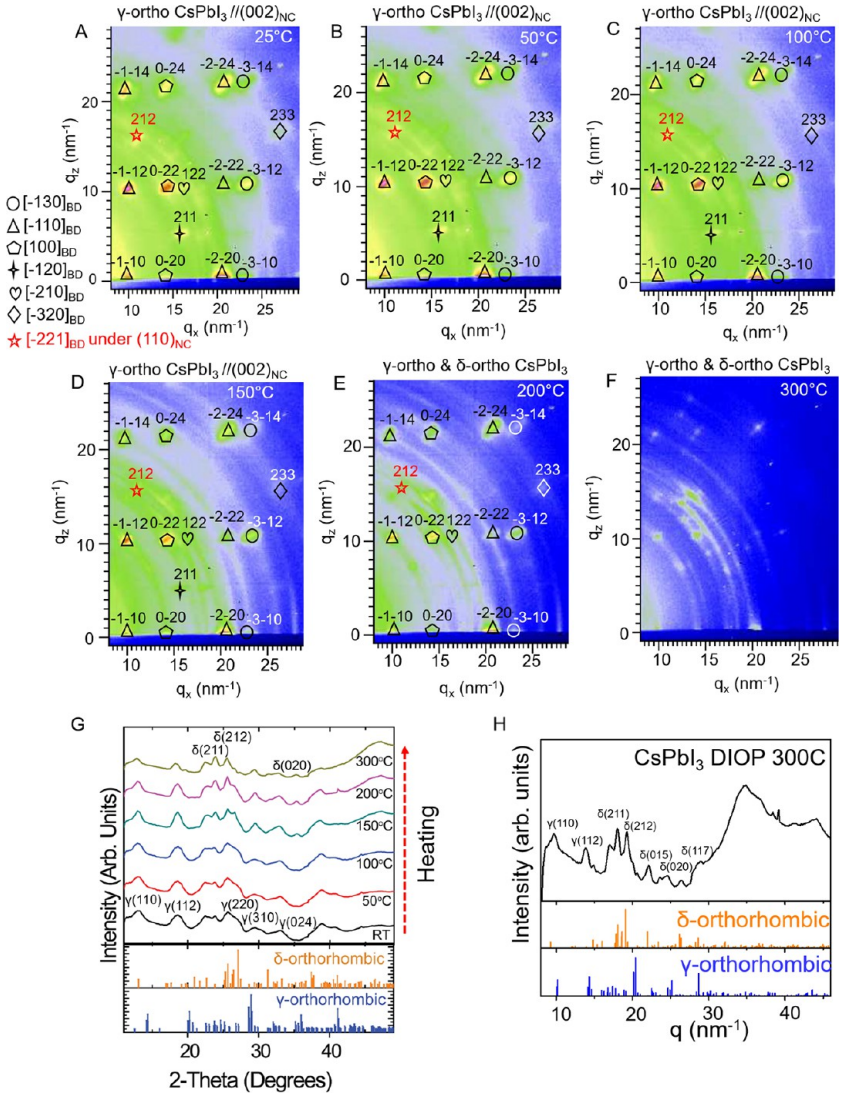

Figure 5. (A–F) GIWAXS data for superlattices of $CsPbI_3$ nanocrystals made with OAm and DIOP with in situ heating. The patterns are indexed to the γ-orthorhombic phase with the $\gamma(002)$ planes oriented parallel to the substrate. BD indicates the beam direction corresponding to the peak indexing. (G) Radial integration of the GIWAXS pattern in (A–F). (H) Radial integration of the GIWAXS pattern in (F).

Figure 8, for example, in the photographs of a film of nanocrystals made with OAm and OA being heated under atmospheric conditions. Photographs of the same film before and after heating under room light and UV light are provided as the Supporting Information in Figure S7. The film begins to turn yellow at ~200 °C and has become completely yellow by 250 °C. The film's reddish appearance at room temperature results from its bright red fluorescence. As the temperature increases, the film becomes increasingly black because the PL is decreasing. The red hue has disappeared by about 100 °C. This is also observed from films of nanocrystals made with OAm and DIOP. PL spectra and images of the films of γ-$CsPbI_3$ nanocrystals made with OAm and DIOP heated on a glass substrate are provided as the Supporting Information in Figures S8 and S9.

The PL emission peak also shifts to a longer wavelength as the temperature increases. Schaller's group[38] recently reported the PL spectra of $CsPbI_3$ nanocrystals embedded in a polymer film heated from 25 to 230 °C and found that the peak wavelength did not noticeably change during heating. This would indicate that in our case there may be enhanced electronic coupling between neighboring nanocrystals that occur in the superlattice upon heating that could be responsible for the observed red shift in PL.[35]

Upon heating, there is also some weak light emission observed from δ-$CsPbI_3$. This is the asymmetric PL peak at 440 nm that becomes visible once the temperature reaches 170 °C. This peak eventually dominates the PL spectra when the temperature reaches 230 °C. The weak light emission from δ-$CsPbI_3$ remains after cooling the sample back to 25 °C. Similar PL signatures have been observed for yellow δ-$CsPbI_3$ nanowires.[39]

We also heated films of $CsPbI_3$ nanocrystals under nitrogen to determine how important humidity and air are to determining the temperature of the γ-to-δ phase transition of the nanocrystals. Photographs of the heated films are provided as the Supporting Information in Figures S10 and S11. $CsPbI_3$ nanocrystals made with OAm and OA begin to turn yellow at ~225 °C, which is about 25 °C higher than when heated in humid air. The film becomes completely yellow when the temperature reaches 300 °C. $CsPbI_3$ nanocrystals made with OAm and DIOP begin to turn yellow at ~205 °C, which is the same temperature as when heated in humid air. Similar to the

DOI: 10.1021/acs.chemmater.9b03533
Chem. Mater. 2019, 31, 9750–9758

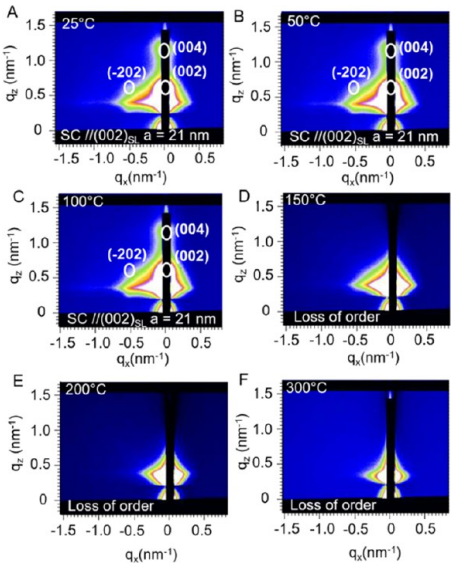

Figure 6. GISAXS of superlattices of $CsPbI_3$ nanocrystals made with OAm and DIOP with in situ heating at (A) 25 °C, (B) 50 °C, (C) 100 °C, (D) 150 °C, (E) 200 °C, and (F) 300 °C. Diffraction spots are indexed to a simple cubic (SC) superlattice with lattice parameter a_{SL} = 21 nm with a $(001)_{SL}$ orientation on the substrate.

OAm/OA nanocrystal films, the OAm/DIOP film has turned completely yellow by 300 °C. It appears that humidity plays a relatively minor role in catalyzing the γ-to-δ phase transition of heated ligand-stabilized nanocrystals. The retention of the γ-phase of $CsPbI_3$ nanocrystals is largely determined by the thermal stability of the ligand bonding to the nanocrystal surface, similar to many other types of nanocrystals. For example, alkanethiol-capped gold nanocrystals sinter when the temperature reaches only ~190 °C because of the degradation of the Au−S bond. In the case of the gold nanocrystals, chemical species like halides can also catalyze the destabilization of the ligand layer on the nanocrystal surface at slightly lower temperatures.[36] Future detailed kinetic studies of the thermally induced γ-to-δ phase transition in $CsPbI_3$ nanocrystals will reveal more information about how different ligands and chemical species in the environment affect the stability of the black phase.

CONCLUSIONS

Uniform cube-shaped nanocrystals of $CsPbI_3$ exhibiting the black phase were synthesized, assembled into superlattices, and studied using GISAXS, GIWAXS, and PL spectroscopy with in situ heating. The cube-shaped nanocrystals assemble into simple cubic superlattices with nanocrystals depositing on the substrate on their faceted surfaces, leading to a strongly preferred crystal orientation on the substrate. This enables GIWAXS to be used to differentiate between the α-cubic and γ-orthorhombic crystal structures, and we find that the nanocrystals inhabit the γ-orthorhombic phase. Heating experiments showed that the black perovskite phase is very stable in ligand-capped $CsPbI_3$ nanocrystals. When heated under atmospheric conditions with relatively high humidity (40%), the γ-to-δ phase transition did not occur until reaching temperatures near 200 °C. Bulk films and crystals of black $CsPbI_3$ change nearly instantaneously to the yellow δ-orthorhombic phase when exposed to moisture at room temperature.[40] The significant stability of the non-equilibrium perovskite phase of $CsPbI_3$ comes primarily from the protective ligand shell that prevents water vapor from reaching the $CsPbI_3$ surface and catalyzing the phase transformation. There is probably also a stabilizing effect from the nanometer size of the crystals, as others have also suggested.[15] The difference

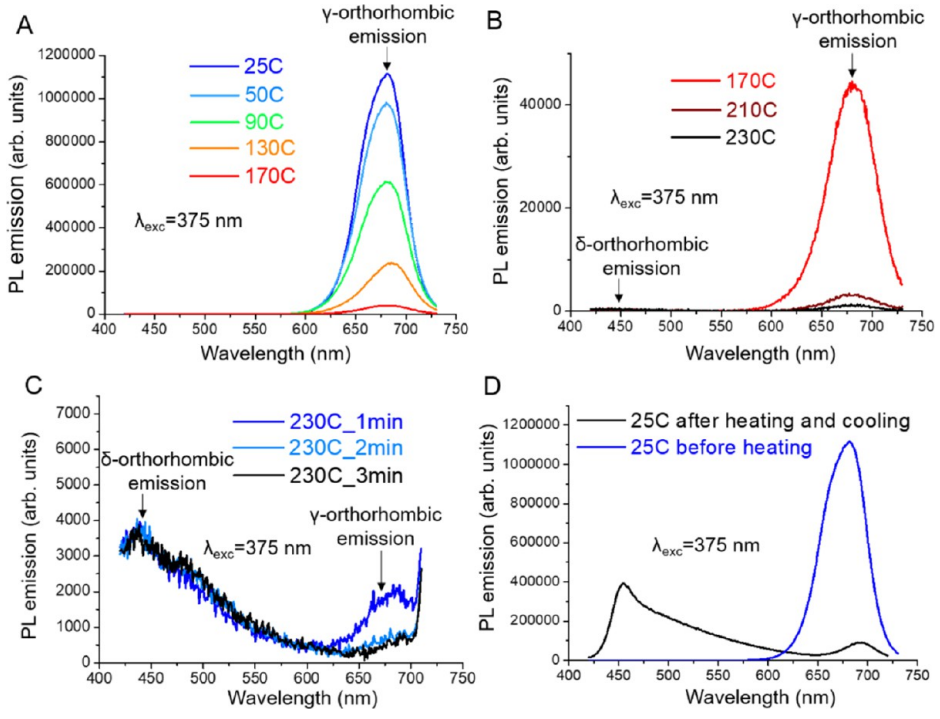

Figure 7. (A−D) In situ PL emission spectra (λ_{exc} = 375 nm) of a film of γ-$CsPbI_3$ nanocrystals synthesized with OAm and OA heated on a glass slide in humid air (RH = 42%). The spectra in (A−C) are measured using the same slit size with similar data acquisition times, and the intensity is plotted to scale. In (D), the spectrum of 25 °C before heating is measured under slit size 2, and 25 °C after heating is under slit size 5. The emission of δ-orthorhombic phase[39] at ~440 nm is visible starting from 170 °C, becomes dominant at 230 °C, and remains after cooling down to 25 °C.

DOI: 10.1021/acs.chemmater.9b03533
Chem. Mater. 2019, 31, 9750−9758

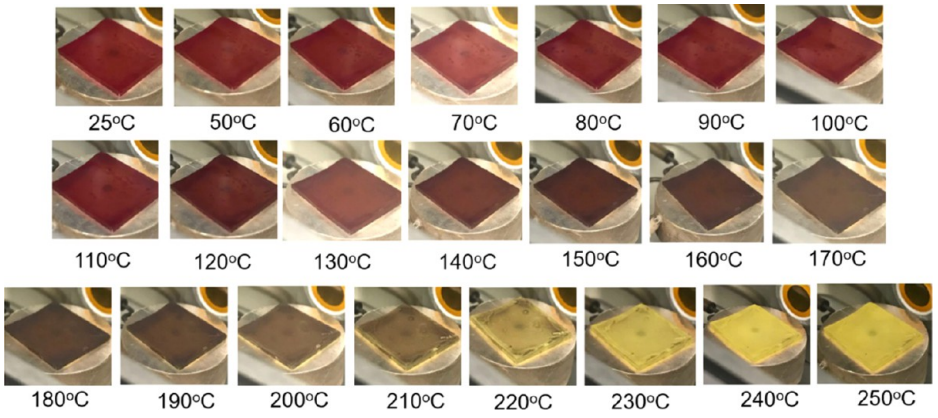

Figure 8. Photographs of a film of γ-$CsPbI_3$ nanocrystals made with OAm and OA being heated in humid air (RH = 42%) on a glass substrate (1 cm × 1 cm). The film is heated at 10 °C min^{-1}. The yellow color begins to develop at 200 °C, and by reaching 250 °C, the entire film is yellow.

in stability between nanocrystals synthesized with OAm and OA or DIOP is not very noticeable, although there do appear to be subtle differences in the kinetics of the transition that depend on the ligand shell chemistry. This topic requires further study with more detailed measurements of the rates of the phase transition at different temperatures.

■ ASSOCIATED CONTENT

Supporting Information

The Supporting Information is available free of charge at https://pubs.acs.org/doi/10.1021/acs.chemmater.9b03533.

Indexation details for the room temperature GIWAXS data in Figure 2; indexation for the 200 and 300 °C GIWAXS data in Figures 3E,F and 5F; TGA of $CsPbI_3$ nanocrystals; SEM images of $CsPbI_3$ nanocrystals heated to 190 °C in humid air; in situ PL emission spectra and photographs of films of $CsPbI_3$ nanocrystals heated on glass in humid air; photographs of films of $CsPbI_3$ nanocrystals being heated on glass in nitrogen (PDF)

Video of a $CsPbI_3$ nanocrystal film that is heated in air and then cooled back to room temperature (MP4)

Videos of 2D GIWAXS patterns with in situ heating in air of superlattices of $CsPbI_3$ nanocrystals made with OAm and OA or DIOP (MP4)(MP4)

■ AUTHOR INFORMATION

Corresponding Author

*E-mail: korgel@che.utexas.edu. Tel: +1-512-471-5633. Fax: +1-512-471-7060.

ORCID

Yangning Zhang: 0000-0001-5511-955X
Francis Leonard Deepak: 0000-0002-3833-1775
Detlef-M. Smilgies: 0000-0001-9351-581X
Delia J. Milliron: 0000-0002-8737-451X
Brian A. Korgel: 0000-0001-6242-7526

Author Contributions

⊥C.J.T. and Y.Z. contributed equally to this work.

Notes

The authors declare no competing financial interest.

■ ACKNOWLEDGMENTS

This work was funded by the Robert A. Welch Foundation (grant nos. F-1464 and F-1848), the NSF Industry/University Cooperative Research Center on Next Generation Photovoltaics (IIP-1540028, IIP-1624539, IIP-1822206), and the Center for Dynamics and Control of Materials (CDCM) Materials Research Science and Engineering Center (MRSEC) supported by the NSF (DMR-1720595). C.J.T. acknowledges financial support from the National Science Foundation through its Graduate Research Fellowship Program (grant no. DGE-1610403). The Cornell High Energy Synchrotron Source (CHESS) is a national user facility supported by the National Science Foundation under award DMR-1332208. The authors also acknowledge support through the UT@INL Corner, as part of the UT|Portugal program.

■ REFERENCES

(1) Kojima, A.; Teshima, K.; Shirai, Y.; Miyasaka, T. Organometal Halide Perovskites as Visible-Light Sensitizers for Photovoltaic Cells. *J. Am. Chem. Soc.* **2009**, *131*, 6050−6051.

(2) Im, J.-H.; Lee, C.-R.; Lee, J.-W.; Park, S.-W.; Park, N.-G. 6.5% Efficient Perovskite Quantum-Dot Sensitized Solar Cell. *Nanoscale* **2011**, *3*, 4088.

(3) Lee, M. M.; Teuscher, J.; Miyasaka, T.; Murakami, T. N.; Snaith, H. J. Efficient Hybrid Solar Cells Based on Meso-Superstructured Organometal Halide Perovskites. *Science* **2012**, *338*, 643−648.

(4) NREL Efficiency Chart. https://www.nrel.gov/pv/cell-efficiency.html (retrieved November 4, 2019).

(5) Tan, Z.-K.; Moghaddam, R. S.; Lai, M. L.; Docampo, P.; Higler, R.; Deschler, F.; Price, M.; Sadhanala, A.; Pazos, L. M.; Credgington, D.; Hanusch, F.; Bein, T.; Snaith, H. J.; Friend, R. H. Bright Light-Emitting Diodes Based on Organometal Halide Perovskite. *Nat. Nanotechnol.* **2014**, *9*, 687−692.

(6) Eperon, G. E.; Paterno, G. M.; Sutton, R. J.; Zampetti, A.; Haghighirad, A. A.; Cacialli, F.; Snaith, H. J. Inorganic Caesium Lead Iodide Perovskite Solar Cells. *J. Mater. Chem. A* **2015**, *3*, 19688−19695.

(7) Wang, K.; Jin, Z.; Liang, L.; Bian, H.; Bai, D.; Wang, H.; Zhang, J.; Wang, Q.; Liu, S. All-Inorganic Cesium Lead Iodide Perovskite Solar Cells with Stabilized Efficiency Beyond 15%. *Nat. Commun.* **2018**, *9*, No. 4544.

(8) Wang, Y.; Dar, M. I.; Ono, L. K.; Zhang, T.; Kan, M.; Li, Y.; Zhang, L.; Wang, X.; Yang, Y.; Gao, X.; Qi, Y.; Grätzel, M.; Zhao, Y. Thermodynamically Stabilized β-$CsPbI_3$-Based Perovskite Solar Cells with Efficiencies>18%. *Science* **2019**, *365*, 591−595.

(9) Eperon, G. E.; Leitjens, T.; Bush, K. A.; Prasanna, R.; Green, T.; Wang, J. T.-W.; McMeekin, D. P.; Volonakis, G.; Milot, R. L.; May, R.; Palmstrom, A.; Slotcavage, D. J.; Belisle, R. A.; Patel, J. B.; Parrott, E. S.; Sutton, R. J.; Ma, W.; Moghadam, F.; Conings, B.; Babayigit, A.; Boyen, H.-G.; Bent, S.; Giustino, F.; Herz, L. M.; Johnston, M. B.; McGehee, M. D.; Snaith, H. J. Perovskite-Perovskite Tandem

DOI: 10.1021/acs.chemmater.9b03533
Chem. Mater. 2019, 31, 9750−9758

Photovoltaics with Optimized Band Gaps. *Science* **2016**, *354*, 861−865.
(10) Leijtens, T.; Bush, K. A.; Prasanna, R.; McGehee, M. D. Opportunities and Challenges for Tandem Solar Cells Using Metal Halide Perovskite Semiconductors. *Nat. Energy* **2018**, *3*, 828−838.
(11) Beal, R. E.; Slotcavage, D. J.; Leijtens, T.; Bowring, A. R.; Belisle, R. A.; Nguyen, W. H.; Burkhard, G. F.; Hoke, E. T.; McGeheee, M. D. Cesium Lead Halide Perovskites with Improved Stability for Tandem Solar Cells. *J. Phys. Chem. Lett.* **2016**, *7*, 746−751.
(12) Dastidar, S.; Hawley, C. J.; Dillon, A. D.; Gutierrez-Perez, A. D.; Spaneir, J. E.; Fafarman, A. T. Quantitative Phase-Change Thermodynamics and Metastability of Perovskite-Phase Cesium Lead Halide. *J. Phys. Chem. Lett.* **2017**, *8*, 1278−1282.
(13) Marronnier, A.; Roma, G.; Boyer-Richard, S.; Pedesseau, L.; Jancu, J.-M.; Bonnassieux, Y.; Katan, C.; Stoumpos, C. C.; Kanatzidis, M. G.; Even, J. Anharmonicity and Disorder in the Black Phases of Cesium Lead Iodide Used for Stable Inorganic Perovskite Solar Cells. *ACS Nano* **2018**, *12*, 3477−3486.
(14) Sutton, R. J.; Filip, M. R.; Haghighirad, A. A.; Sakai, N.; Wenger, B.; Giustino, F.; Snaith, H. J. Cubic or Orthorhombic? Revealing the Crystal Structure of Metastable Black-Phase $CsPbI_3$ by Theory and Experiment. *ACS Energy Lett.* **2018**, *3*, 1787−1794.
(15) Zhao, B.; Jin, S.-F.; Huang, S.; Liu, N.; Ma, J.-Y.; Xue, D.-J.; Han, Q.; Ding, J.; Ge, Q.-Q.; Feng, Y.; Hu, J.-S. Thermodynamically Stable Orthorhombic γ-$CsPbI_3$ Thin Films for High-Performance Photovoltaics. *J. Am. Chem. Soc.* **2018**, *140*, 11716−11725.
(16) Straus, D. B.; Guo, S.; Cava, R. J. Kinetically Stable Single Crystals of Perovskite-Phase $CsPbI_3$. *J. Am. Chem. Soc.* **2019**, *141*, 11435−11439.
(17) Tai, Q.; Tang, K.-C.; Yan, F. Recent Progress of Inorganic Perovskite Solar Cells. *Energy Environ. Sci.* **2019**, *12*, 2375−2405.
(18) Swarnkar, A.; Marshall, A. R.; Sanehira, E. M.; Chernomordik, B. D.; Moore, D. T.; Christians, J. A.; Chakrabarti, T.; Luther, J. M. Quantum Dot-Induced Phase Stabilization of α-$CsPbI_3$ Perovskite for High-Efficiency Photovoltaics. *Science* **2016**, *354*, 92−95.
(19) Protesescu, L.; Yakunin, S.; Bodnarchuk, M. I.; Krieg, F.; Caputo, R.; Hendon, C. H.; Yang, R. X.; Walsh, A.; Kovalenko, M. V. Nanocrystals of Cesium Lead Halide Perovskites ($CsPbX_3$, X=Cl, Br, and I): Novel Optoelectronic Materials Showing Bright Emission with Wide Color Gamut. *Nano Lett.* **2015**, *15*, 3692−3696.
(20) Sanehira, E. M.; Marshall, A. R.; Christians, J. A.; Harvey, S. P.; Ciesielki, P. N.; Wheeler, L. M.; Schulz, P.; Lin, L. Y.; Beard, M. C.; Luther, J. M. Enhanced Mobility $CsPbI_3$ Quantum Dot Arrays for Record-Efficiency, High-Voltage Photovoltaic Cells. *Sci. Adv.* **2017**, *3*, No. eaao4204.
(21) Wu, T.; Wang, Y.; Dai, Z.; Cui, D.; Wang, T.; Meng, X.; Bi, E.; Yang, X.; Han, L. Efficient and Stable $CsPbI_3$ Solar Cells via Regulating Lattice Distortion with Surface Organic Terminal Groups. *Adv. Mater.* **2019**, *31*, No. 1900605.
(22) Wang, K.; Jin, Z.; Liang, L.; Bian, H.; Wang, H.; Feng, J.; Wang, Q.; Liu, S. Chlorine Doping for Black γ-$CsPbI_3$ Solar Cells with Stabilized Efficiency Beyond 16%. *Nano Energy* **2019**, *58*, 175−182.
(23) Ma, S.; Kim, S. H.; Jeong, B.; Kwon, H.-C.; Yun, S.-C.; Jang, G.; Yang, H.; Park, C.; Lee, D.; Moon, J. Strain-Mediated Phase Stabilization: A New Strategy for Ultrastable α-$CsPbI_3$ Perovskite by Nanoconfined Growth. *Small* **2019**, *15*, No. 1900219.
(24) Liang, L.; Liu, M.; Jin, Z.; Wang, Q.; Wang, H.; Bian, H.; Shi, F.; Liu, S. Optical Management with Nanoparticles for a Light Conversion Efficiency Enhancement in Inorganic γ-$CsPbI_3$ Solar Cells. *Nano Lett.* **2019**, *19*, 1796−1804.
(25) Becker, P.; Márquez, J. A.; Just, J.; Al-Ashouri, A.; Hages, C.; Hempel, H.; Jošt, M.; Albrecht, S.; Frahm, R.; Unold, T. Low Temperature Synthesis of Stable γ-$CsPbI_3$ Perovskite Layer for Solar Cells Obtained by High Throughput Experimentation. *Adv. Energy Mater.* **2019**, *9*, No. 1900555.
(26) Liu, F.; Ding, C.; Zhang, Y.; Kamisaka, T.; Zhao, Q.; Luther, J. M.; Toyoda, T.; Hayase, S.; Minemoto, T.; Yoshino, K.; Zhang, B.; Dai, S.; Jiang, J.; Tao, S.; Shen, Q. GeI_2 Additive for High Optoelectronic Quality $CsPbI_3$ Quantum Dots and Their Application in Photovoltaic Devices. *Chem. Mater.* **2019**, *31*, 798−807.
(27) Ye, Q.; Zhao, Y.; Mu, S.; Gao, P.; Zhang, X.; You, J. Stabilizing the Black Phase of Cesium Lead Halide Inorganic Perovskite for Efficient Solar Cells. *Sci. China Chem.* **2019**, *62*, 810−821.
(28) Mir, W. J.; Swarnkar, A.; Nag, A. Postsynthesis Mn-Doping in $CsPbI_3$ Nanocrystals to Stabilize The Black Perovskite Phase. *Nanoscale* **2019**, *11*, 4278−4286.
(29) Suri, M.; Hazarika, A.; Larson, B. W.; Zhao, Q.; Valles-Pelarda, M.; Siegler, T. D.; Abney, M. K.; Ferguson, A. J.; Korgel, B. A.; Luther, J. M. Enhanced Open-Circuit Voltage of Wide-Bandgap Perovskite Photovoltaics by Using Alloyed $(FA_{1-x}Cs_x)Pb(I_{1-x}Br_x)_3$ Quantum Dots. *ACS Energy Lett.* **2019**, *4*, 1954−1960.
(30) Wang, C.; Chesman, A. S. R.; Jasieniak, J. J. Stabilizing the Cubic Perovskite Phase of $CsPbI_3$ Nanocrystals by Using an Alkyl Phosphinic Acid. *Chem. Commun.* **2017**, *53*, 232−235.
(31) Smilgies, D.; Blasini, D. R. Indexation Scheme for Oriented Molecular Thin Films Studied with Grazing-Incidence Reciprocal-Space Mapping. *J. Appl. Crystallogr.* **2007**, *40*, 716−718.
(32) Yu, Y.; Lu, X.; Guillaussier, A.; Reddy Voggu, V.; Pineros, W.; de la Mata, M.; Arbiol, J.; Smilgies, D.-M.; Truskett, T. M.; Korgel, B. A. Orientationally Ordered Silicon Nanocrystal Cuboctahedra in Superlattices. *Nano Lett.* **2016**, *16*, 7814−7821.
(33) Zhang, Y.; Thomas, C. J.; Guillaussier, A.; Smilgies, D.-M.; Korgel, B. A. Thermal Phase Transitions in Superlattice Assemblies of Cuboidal $CH_3NH_3PbI_3$ Nanocrystals Followed by Grazing Incidence X-ray Scattering. *J. Phys. Chem. C* **2019**, *123*, 17555−17565.
(34) Zhang, Y.; Shah, T.; Deepak, F. L.; Korgel, B. A. Surface Science and Colloidal Stability of Double Perovskite $Cs_2AgBiBr_6$ Nanocrystals and their Superlattices. *Chem. Mater.* **2019**, *31*, 7962−7969.
(35) Nagaoka, Y.; Hills-Kimball, K.; Tan, R.; Li, R.; Wang, Z.; Chen, O. Nanocube Superlattices of Cesium Lead Bromide Perovskites and Pressure-Induced Phase Transformations at Atomic and Mesoscale Levels. *Adv. Mater.* **2017**, *29*, No. 1606666.
(36) Yu, Y.; Goodfellow, B. W.; Rasch, M. R.; Bosoy, C.; Smilgies, D.-M.; Korgel, B. A. Role of Halides in the Ordered Structure Transitions of Heated Gold Nanocrystal Superlattices. *Langmuir* **2015**, *31*, 6924−6932.
(37) Goodfellow, B. W.; Patel, R. N.; Panthani, M. G.; Smilgies, D.-M.; Korgel, B. A. Melting and Sintering of a Body-Centered Cubic Superlattice of PbSe Nanocrystals Followed by Small Angle X-ray Scattering. *J. Phys. Chem. C* **2011**, *115*, 6397−6404.
(38) Diroll, B. T.; Nedelcu, G.; Kovalenko, M. V.; Schaller, R. D. High-Temperature Photoluminescence of $CsPbX_3$(X = Cl, Br, I) Nanocrystals. *Adv. Funct. Mater.* **2017**, *27*, No. 1606750.
(39) Lai, M.; Kong, Q.; Bischak, C. G.; Yu, Y.; Dou, L.; Eaton, S. W.; Ginsberg, N. S.; Yang, P. Structural, Optical, and Electrical Properties of Phase-Controlled Cesium Lead Iodide Nanowires. *Nano Res.* **2017**, *10*, 1107−1114.
(40) Burwig, T.; Fränzel, W.; Pistor, P. Crystal Phases and Thermal Stability of Co-evaporated $CsPbX_3$ (X = I, Br) Thin Films. *J. Phys. Chem. Lett.* **2018**, *9*, 4808−4813.

DOI: 10.1021/acs.chemmater.9b03533
Chem. Mater. 2019, 31, 9750−9758